LETTER

doi:10.1038/nature12139

Crystal structure of a nitrate/nitrite exchanger

Hongjin Zheng[1], Goragot Wisedchaisri[1] & Tamir Gonen[1]

Mineral nitrogen in nature is often found in the form of nitrate (NO_3^-). Numerous microorganisms evolved to assimilate nitrate and use it as a major source of mineral nitrogen uptake[1]. Nitrate, which is central in nitrogen metabolism, is first reduced to nitrite (NO_2^-) through a two-electron reduction reaction[2,3]. The accumulation of cellular nitrite can be harmful because nitrite can be reduced to the cytotoxic nitric oxide. Instead, nitrite is rapidly removed from the cell by channels and transporters, or reduced to ammonium or dinitrogen through the action of assimilatory enzymes[3]. Despite decades of effort no structure is currently available for any nitrate transport protein and the mechanism by which nitrate is transported remains largely unknown. Here we report the structure of a bacterial nitrate/nitrite transport protein, NarK, from *Escherichia coli*, with and without substrate. The structures reveal a positively charged substrate-translocation pathway lacking protonatable residues, suggesting that NarK functions as a nitrate/nitrite exchanger and that protons are unlikely to be co-transported. Conserved arginine residues comprise the substrate-binding pocket, which is formed by association of helices from the two halves of NarK. Key residues that are important for substrate recognition and transport are identified and related to extensive mutagenesis and functional studies. We propose that NarK exchanges nitrate for nitrite by a rocker switch mechanism facilitated by inter-domain hydrogen bond networks.

The nitrate/nitrite porter (NNP) family of membrane proteins evolved to efficiently translocate the ionic molecules NO_3^- and NO_2^- across the membrane[4,5]. Two nitrate/nitrite transport proteins NarK and NarU were identified in *Escherichia coli*[6–10]. NarK proteins have been shown to catalyse either nitrate/nitrite exchange or nitrate uptake, presumably by symport with a proton[1,9,10]. The former activity would be associated with respiration, whereas the latter could be associated either with respiration or the net assimilation of nitrite into cell material. (An additional membrane protein, NirC, functions as a H^+/nitrite channel in *E. coli* but is not a member of the NNP[10].) Nitrate is the preferred source of nitrogen for plants and at least 16 nitrate/nitrite transport proteins have been identified[11]. In plants the function of NNP proteins is probably related solely to the net assimilation of nitrogen.

The NNP family belongs to the major facilitator superfamily (MFS) of secondary transporters. MFS members show specificity to a wide range of molecules[12]. Although more than 58 distinct families of transporters make up the MFS, representatives of only six such families have been crystallized and their structure determined[13–19]. These six representative transporters require protons for their function. All MFS members are postulated to function through the rocker switch mechanism[12]. They all share a common structural topology, but share little or no sequence homology.

Here we report the first crystal structure of a nitrate transport protein that also transports nitrite. The structure of the *E. coli* NarK with and without substrate was determined by X-ray crystallography. Functionally important residues that form the substrate-binding pocket are identified and related to previously described mutagenesis and functional studies. We provide the first evidence that NarK functions as a nitrate/nitrite exchanger, and that protons are probably not co-transported with the substrate.

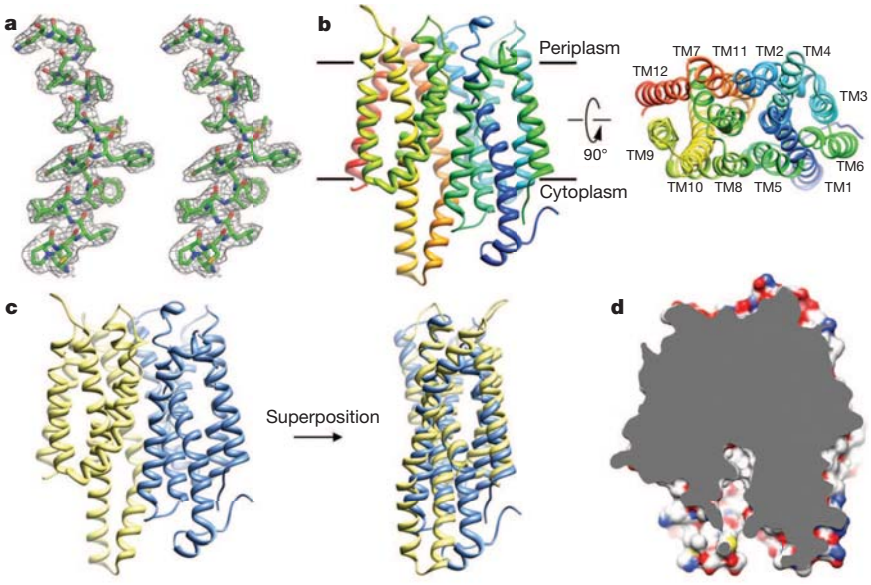

Figure 1 | The crystal structure of NarK. **a**, Part of TM2 of NarK is shown in stereo view with a sigmA-weighted $2F_o - F_c$ map at 2.6 Å resolution, contoured at 1.0σ. **b**. Left, NarK structure viewed from the plane of membrane with the putative location of the lipid bilayer as indicated. NarK is coloured in rainbow with the N terminus in blue. Right, NarK viewed from the periplasmic side. The identity of the 12 transmembrane helices is indicated. **c**, The N-terminal domain (TM1–TM6) of NarK (blue) is pseudo-symmetric to the C-terminal domain (TM7–TM12) (yellow) and can be superimposed with an r.m.s.d. of 2.9 Å. **d**, Cut-away surface representation of the inward-facing NarK shows the central cavity exposed to the cytosol.

[1]Janelia Farm Research Campus, Howard Hughes Medical Institute, 19700 Helix Drive, Ashburn, Virginia 20147, USA.

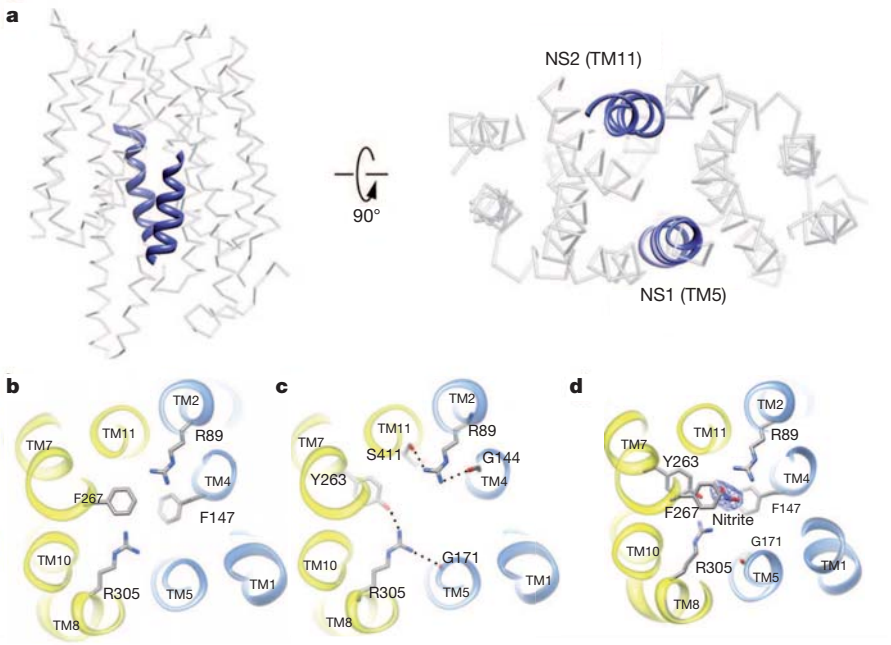

Figure 2 | The substrate-binding site in NarK. **a**, Two highly conserved nitrate signature motifs in TM5 and TM11 (blue helices) at the centre of NarK form the nitrate/nitrite transport pathway. **b**, The substrate-binding pocket is defined by two evolutionarily conserved and functionally important arginine residues R89 and R305. The binding site is capped above and below by F267 and F147, respectively. **c**, R89 and R305 are stabilized by inter-domain hydrogen bonds as depicted. The two halves of NarK are indicated as blue (N-terminal domain) and yellow (C-terminal domain). **d**, Nitrite-bound structure of NarK. The density for nitrite is observed at the substrate-binding site after soaking the NarK crystals with sodium nitrite. R305 undergoes a conformational change upon substrate binding. This conformational change affects the inter-domain network of hydrogen bonds between Y263, G171 and R305. The displayed map is a sigmaA-weighted $F_o - F_c$ at 3σ.

We overexpressed NarK, and purified the protein to homogeneity as described in the Methods section. Well-ordered high-quality crystals were obtained when NarK was co-crystallized with the Fab fragment of a monoclonal antibody we developed. The data extended to 2.6 Å were phased using molecular replacement with Fab as a search model. The resulting density map was of high enough quality, allowing us to build and refine the NarK structure (Fig. 1a). The asymmetric unit contains one molecule of NarK forming a complex with one molecule of Fab (Supplementary Fig. 1). NarK, as other MFS proteins, is structurally divided into two domains, the amino-terminal half and the carboxy-terminal half each consisting of six transmembrane helices (TM1–TM6 and TM7–TM12, respectively) (Fig. 1b, c). The two domains are connected by a long loop between TM6 and TM7 (disordered in our structure), and it is thought that the substrate transport pathway is localized at the interface between these two domains. NarK appears to be in the inward-facing conformation as the hydrophilic central cavity is exposed to the cytosolic side (Fig. 1d). A detailed description of the crystal packing and the overall architecture of NarK can be found in the Supplementary Information.

All members of the NNP family contain two stretches of conserved residues called the nitrate signature (NS) motifs (Supplementary Fig. 2). The nitrate signature motifs are not found in other MFS members, but are a unique feature of the NNP family[20]. In NarK, the NS1 motif is formed by residues 164–175 (GGALGLNGGLGN) located on TM5. The NS2 motif of NarK is formed by residues 408–420 (GFISAIGAIGGFF) located on TM11 (Fig. 2a, blue). The nitrate signature motifs in NarK are located at the centre of the protein, lining part of the substrate transport pathway (Fig. 2a, right). Both of the nitrate signature motifs are glycine-rich, which ensures a tight fit among the surrounding helices. The result is a significantly more compact structure for NarK when compared to other known structures of MFS members (Supplementary Fig. 3).

To transport anions like NO_3^- and NO_2^-, polar residues lining the central pore are most likely to form the substrate-binding pocket and be involved in substrate recognition and transport. Two arginine residues, R89 from TM2 and R305 from TM8, are absolutely conserved among all nitrate/nitrite transporters in both prokaryotes and eukaryotes (Supplementary Fig. 2). Structurally, R89 and R305 are in plane and appose one another at the very centre of NarK, with their side chains extending well into the central cavity of the transporter (Fig. 2b). These arginines are capped by two phenylalanine residues: F267 above and F147 below. Together the arginines and the phenylalanines form the substrate-binding pocket. The only bulky side chain in plane with the arginines is Y263, which forms a hydrogen bond with R305 (Fig. 2c). The two arginine side chains are stabilized by an intricate system of inter-domain hydrogen bonds that link the two halves of NarK (Fig. 2c). Mutation of the residues described above led to a complete loss of function in NarK and its close homologues (Supplementary Fig. 2

Table 1 | Mutagenesis and functional study of key residues important for nitrate/nitrite exchange

NarK (*E. coli*)	NarU (*E. coli*)	NrtA (*Aspergillus nidulans*)	Colony growth on nitrate
R89	R87K*	R87K†	+
	R87P*	R87T†	–
N175		N168A‡	–
		N168Q†	–
		N168C†	–
Y263	Y261Q*		+
	Y261N*		+
R305	R303Q*	R368K†	+
	R303C*	R368Q†	–
		R368C†	–
A415		N459A‡	–
		N459Q†	+
		N459K†	–
		N459C†	–

*Study published in ref. 10.
†Study published in ref. 24.
‡Study published in ref. 21.
See references above for a comprehensive list of all available mutagenesis data.

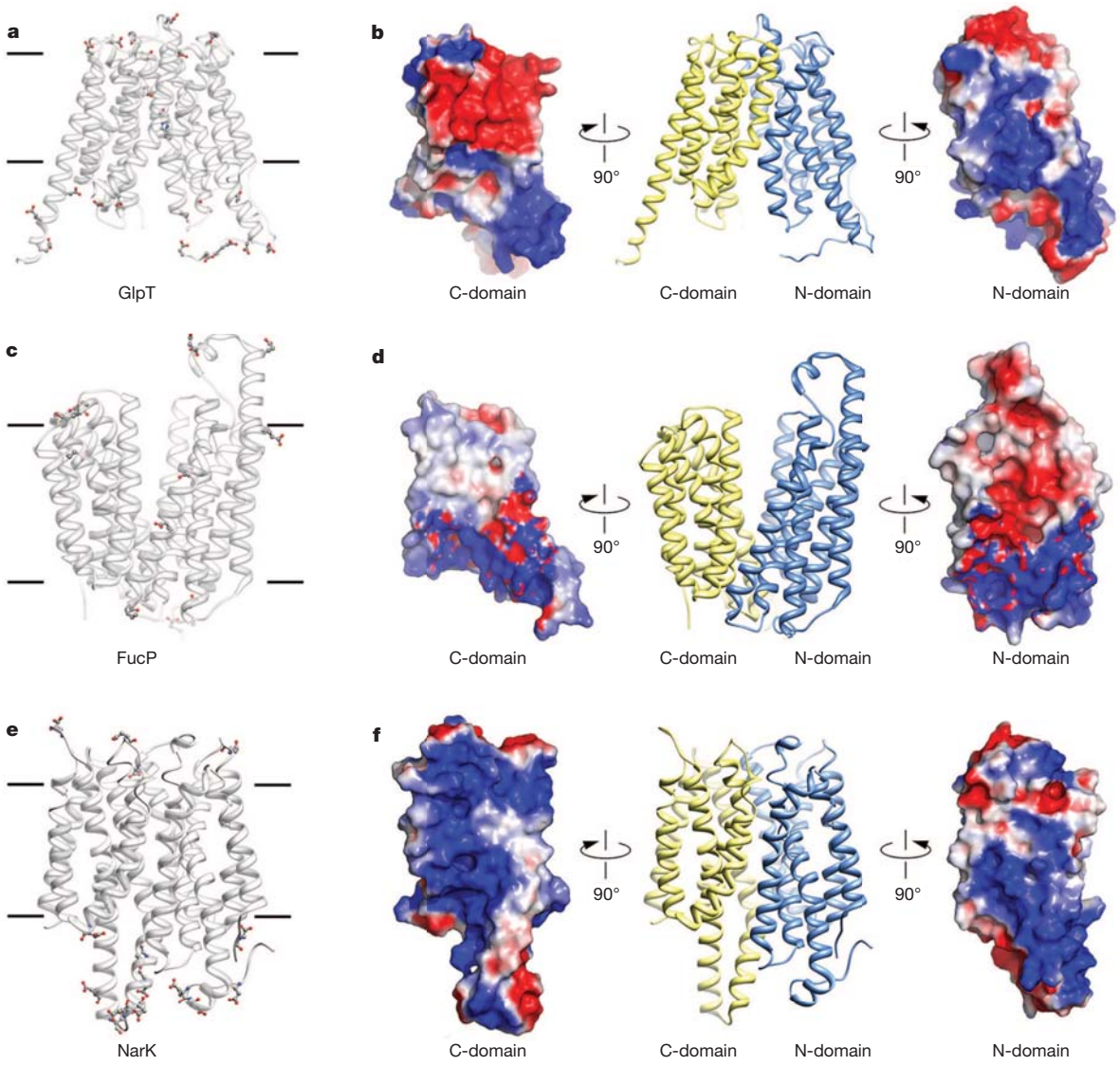

Figure 3 | Protons are probably excluded from the substrate translocation pathway of NarK. **a**, Location of histidine, aspartate and glutamate residues in the anion transporter GlpT. Acidic residues line the substrate translocation pathway. **b**, Electrostatic surface representation for each domain of GlpT showing a relatively even distribution of positive and negative charges in the substrate translocation pathway. **c**, Location of histidine, aspartate and glutamate residues in the fucose transporter FucP. Acidic residues line the substrate translocation pathway. **d**, Electrostatic surface representation for each domain of FucP. **e**, Location of histidine, aspartate and glutamate residues in NarK. No acidic residues are found in the substrate translocation pathway of NarK. **f**, Electrostatic surface representation for NarK showing a dominantly positively charged substrate translocation pathway. It represents a formidable barrier for the translocation of protons but could attract negatively charged molecules like nitrate and nitrite.

and Table 1). A detailed discussion of the relevant mutational and functional studies can be found in Supplementary Information.

Soaking our NarK crystals with sodium nitrate deteriorated the crystal packing and did not yield meaningful data. In sharp contrast, soaking the crystals with sodium nitrite did not significantly affect crystallinity and yielded data to 2.8 Å resolution (Supplementary Table 1), allowing us to visualize the nitrite bound in the substrate-binding pocket (Fig. 2d and Supplementary Fig. 4). Overall the structure of substrate-free NarK and nitrite-bound NarK are very similar, having an all Cα-atom root mean squared deviation (r.m.s.d.) of 0.6 Å (Supplementary Fig. 5). This is not surprising because NarK is probably stabilized in the inward-facing conformation by crystal contacts and the Fab could further restrict protein movement (Supplementary Fig. 1). Nevertheless, clear densities were observed for nitrite in the substrate-binding pocket (Fig. 2d and Supplementary Fig. 4). Nitrite was observed in-plane with R89 and R305 at the substrate-binding pocket where it is capped above and below by F267 and F147, respectively (Fig. 2d). This binding configuration stabilizes the substrate via the π-electron delocalization among the arginine and phenylalanine side chains. Arginine R305 changed its conformation so that the inter-domain hydrogen bond network involving Y263 and G171 was disrupted upon nitrite binding.

Although it is clear that NarK and other NNP members are capable of NO_3^- uptake and NO_2^- export, it is not clear what the mechanism is or whether the process is proton coupled. Three distinct modes of action have been proposed: H^+/NO_3^- symport, H^+/NO_2^- antiport, or a NO_3^-/NO_2^- exchange without H^+ translocation[1,9,10].

Typically, channels and transporters that translocate protons use residues that are capable of protonation or deprotonation along the pore or substrate pathway[12]. For example, the lactose permease LacY, which co-transports lactose with protons, uses glutamate and histidine residues to translocate the protons[21]. The glycerol-3-phosphate/phosphate antiporter GlpT uses a protonated histidine to facilitate substrate

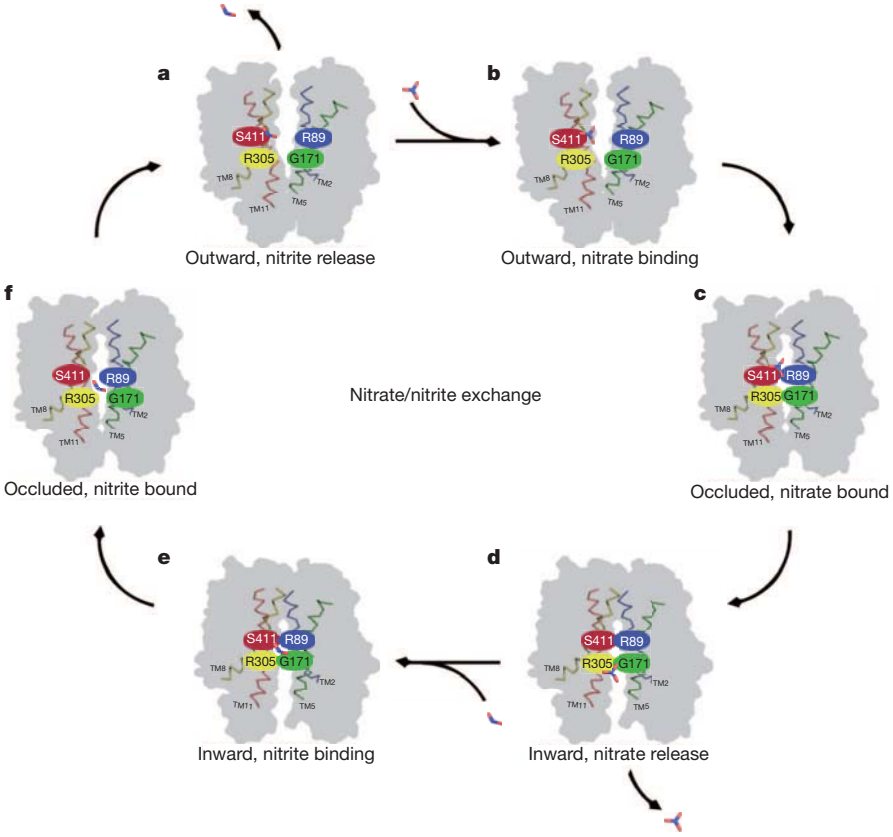

Figure 4 | Proposed mechanism of nitrate/nitrite exchange. **a**–**f**, Six conformations of NarK are depicted as outward facing (**a**), outward facing with nitrate bound (**b**), occluded with nitrate bound (**c**), inward facing with nitrate release (**d**), inward facing with nitrite bound (**e**), occluded with nitrite bound (**f**). Once NarK completes the cycle and returns to the outward facing conformation nitrite is released to the periplasm. The proposed mechanism is based on the rocker switch[12]. For NarK the rocker switch is facilitated by breaking and reforming inter-domain hydrogen bonds involving R89 and R305 as described in Fig. 2.

binding[18] (Fig. 3a, b). The fucose transporter FucP uses glutamates and aspartates to translocate protons together with substrate[16] (Fig. 3c, d). NirC, which is a proton-coupled nitrite channel has a functionally important histidine residue at the centre of the channel[22]. In these four examples, glutamates, aspartates and/or histidines are found on transmembrane helices with their side chains extending into the substrate translocation pathway.

NarK does not contain glutamates, aspartates or histidines on its transmembrane helices. Instead, all glutamates and aspartates are found on either cytoplasmic or periplasmic soluble domains of NarK, well away from the substrate translocation pathway (Fig. 3e, balls and sticks). Moreover, NarK only contains three histidine residues and these are also found on soluble loops. Therefore NarK has no candidate residue for proton translocation or deprotonation in its substrate translocation pathway.

Consistent with the above postulate, surface electrostatic potential calculations in NarK indicate that the substrate translocation pathway is highly positively charged. The electrostatic potentials for the N- and C-terminal halves of NarK are presented in Fig. 3f. The positively charged pathway can facilitate the transport of the negatively charged nitrate and nitrite anions, but at the same time it would represent a formidable barrier for the translocation of protons. In sharp contrast, MFS members that couple the movement of substrate to the movement of protons, have a much more balanced electrostatic distribution in their translocation pathway (Fig. 3). We note that it is possible that protons could be required for NarK activation, but our data indicate that NarK is a nitrate/nitrite exchanger in which protons are not co-transported with the substrate. Moreover, it is still not clear whether NarK could function in nitrite transport alone and if so, whether this could be bidirectional. Further functional studies would have to be performed to answer these questions.

Our data show that NarK functions as a nitrate/nitrite exchanger. We propose the following mechanism for nitrate/nitrite exchange. The mechanism is based on the structural analysis that is presented above, and the previously proposed rocker switch[12] (Fig. 4). Our proposed mechanism of action begins with NarK in the outward conformation in which the substrate translocation pathway is open to the periplasm (Fig. 4a). The positively charged substrate translocation pathway can attract a nitrate molecule, which can enter the pore and bind directly above the two arginines at the substrate-binding site (Fig. 4b and Supplementary Fig. 4). There the nitrate forms hydrogen bonds with R305 and N175 (Fig. 4b). The binding event could then trigger a conformational change in NarK into the transient occluded state where the pore is closed both at the periplasm and cytoplasm (Fig. 4c). The conformational change could push the nitrate from above R89 and R305 to directly below, and as the transporter adopts the inward conformation, its substrate translocation pathway opens to the cytoplasm and nitrate can then be released (Fig. 4d). As nitrate is released it is exchanged with nitrite. Nitrite enters the substrate translocation pathway and binds in plane with R89 and R305 (Figs 2d and 4e). The binding of nitrite at the substrate-binding site triggers the conformational change of NarK from its inward-facing conformation into the outward-facing conformation via the transient occluded state (Fig. 4e, f). During this process nitrite is pushed directly above R89 and R305 and once NarK is facing outward the nitrite is released into the periplasm (Fig. 4a). The cycle of exchange can then continue.

Such a rocker switch mechanism would require a hinge to allow the two halves of NarK to rock against one another as described above. We propose that the hinge is formed by the inter-domain hydrogen bonds involving the conserved arginine residues R89 and R305. As discussed above, these two residues are stabilized by inter-domain hydrogen

bonding: Y263 from the C-terminal domain and G171 from the N-terminal domain of NarK form hydrogen bonds with R305; and G144 of the N-terminal domain and S411 of the C-terminal domain of NarK form hydrogen bonds with R89 (Fig. 2c). As the substrate interacts with R89 and R305, it would disrupt the hydrogen bond networks between the two domains that are mediated by the arginines. Our structure of nitrite-bound NarK indicates that R305 undergoes a conformational change upon substrate binding consistent with a break in the inter-domain hydrogen-bonding network (Fig. 2d). We propose that it is the breaking and reforming of these inter-domain hydrogen bonds through the arginines that allow the two halves of NarK to rock against one another as depicted in Fig. 4. Consistent with this postulate, G171, G144, S411 and Y263 are residues that are conserved in NNP members (Supplementary Fig. 2).

The rocker switch mechanism proposed in other MFS members whose structures are known involves the breaking and the formation of salt bridges and hydrogen bonds between various protein residues[15–19,23]. As discussed above, NarK contains no acidic residues in its pore so salt bridges could only form between protein residues and the substrate, but salt bridges between various protein residues are unlikely to be involved in its mechanism of action. Instead, the pore of NarK is highly positively charged, probably to exclude protons and to attract anions like nitrate and nitrite, whereas the rocking seems to involve the breaking and formation of inter-domain hydrogen bonds at the substrate-binding pocket. It remains to be seen as more structures of MFS members from various families are determined whether other members use a similar pattern of hydrogen bond breaking and formation for their function.

METHODS SUMMARY

NarK from *E. coli* strain K12 was overexpressed in *E. coli* BL21 (DE3) C41. Fab antibody fragments were generated as described in Methods. The NarK–Fab complex was purified in the presence of 0.2% (w/v) *n*-decyl-β-D-maltoside and crystallized in the following condition: 0.1 M citric acid (pH 3.5), 0.1 M NaCl, 0.1 M Li_2SO_4 and 28% PEG400. Nitrite-bound NarK–Fab crystal was obtained by soaking the NarK–Fab crystal in the buffer containing 50 mM sodium nitrite. Diffraction data sets of both crystals were collected at the Advanced Light Source (beamline 8.2.2). Data processing and structure determination were performed using the HKL2000, COOT and CCP4 programs.

Full Methods and any associated references are available in the online version of the paper.

Received 25 September 2012; accepted 2 April 2013.
Published online 12 May 2013.

1. Wood, N. J., Alizadeh, T., Richardson, D. J., Ferguson, S. J. & Moir, J. W. Two domains of a dual-function NarK protein are required for nitrate uptake, the first step of denitrification in *Paracoccus pantotrophus*. *Mol. Microbiol.* **44,** 157–170 (2002).
2. Martínez-Espinosa, R. M., Cole, J. A., Richardson, D. J. & Watmough, N. J. Enzymology and ecology of the nitrogen cycle. *Biochem. Soc. Trans.* **39,** 175–178 (2011).
3. Einsle, O. & Kroneck, P. M. Structural basis of denitrification. *Biol. Chem.* **385,** 875–883 (2004).
4. Saier, M. H. Jr *et al.* Phylogenetic characterization of novel transport protein families revealed by genome analyses. *Biochim. Biophys. Acta* **1422,** 1–56 (1999).
5. Pao, S. S., Paulsen, I. T. & Saier, M. H. Jr. Major facilitator superfamily. *Microbiol. Mol. Biol. Rev.* **62,** 1–34 (1998).
6. Jia, W. & Cole, J. A. Nitrate and nitrite transport in *Escherichia coli*. *Biochem. Soc. Trans.* **33,** 159–161 (2005).
7. DeMoss, J. A. & Hsu, P. Y. NarK enhances nitrate uptake and nitrite excretion in *Escherichia coli*. *J. Bacteriol.* **173,** 3303–3310 (1991).
8. Rowe, J. J., Ubbink-Kok, T., Molenaar, D., Konings, W. N. & Driessen, A. J. NarK is a nitrite-extrusion system involved in anaerobic nitrate respiration by *Escherichia coli*. *Mol. Microbiol.* **12,** 579–586 (1994).
9. Moir, J. W. & Wood, N. J. Nitrate and nitrite transport in bacteria. *Cell. Mol. Life Sci.* **58,** 215–224 (2001).
10. Jia, W., Tovell, N., Clegg, S., Trimmer, M. & Cole, J. A single channel for nitrate uptake, nitrite export and nitrite uptake by *Escherichia coli* NarU and a role for NirC in nitrite export and uptake. *Biochem. J.* **417,** 297–304 (2009).
11. Wang, Y. Y., Hsu, P. K. & Tsay, Y. F. Uptake, allocation and signaling of nitrate. *Trends Plant Sci.* **17,** 458–467 (2012).
12. Law, C. J., Maloney, P. C. & Wang, D. N. Ins and outs of major facilitator superfamily antiporters. *Annu. Rev. Microbiol.* **62,** 289–305 (2008).
13. Sun, L. *et al.* Crystal structure of a bacterial homologue of glucose transporters GLUT1–4. *Nature* **490,** 361–366 (2012).
14. Solcan, N. *et al.* Alternating access mechanism in the POT family of oligopeptide transporters. *EMBO J.* **31,** 3411–3421 (2012).
15. Newstead, S. *et al.* Crystal structure of a prokaryotic homologue of the mammalian oligopeptide-proton symporters, PepT1 and PepT2. *EMBO J.* **30,** 417–426 (2011).
16. Dang, S. *et al.* Structure of a fucose transporter in an outward-open conformation. *Nature* **467,** 734–738 (2010).
17. Yin, Y., He, X., Szewczyk, P., Nguyen, T. & Chang, G. Structure of the multidrug transporter EmrD from *Escherichia coli*. *Science* **312,** 741–744 (2006).
18. Huang, Y., Lemieux, M. J., Song, J., Auer, M. & Wang, D. N. Structure and mechanism of the glycerol-3-phosphate transporter from *Escherichia coli*. *Science* **301,** 616–620 (2003).
19. Abramson, J. *et al.* Structure and mechanism of the lactose permease of *Escherichia coli*. *Science* **301,** 610–615 (2003).
20. Trueman, L. J., Richardson, A. & Forde, B. G. Molecular cloning of higher plant homologues of the high-affinity nitrate transporters of *Chlamydomonas reinhardtii* and *Aspergillus nidulans*. *Gene* **175,** 223–231 (1996).
21. Mirza, O., Guan, L., Verner, G., Iwata, S. & Kaback, H. R. Structural evidence for induced fit and a mechanism for sugar/H^+ symport in LacY. *EMBO J.* **25,** 1177–1183 (2006).
22. Lü, W. *et al.* Structural and functional characterization of the nitrite channel NirC from *Salmonella typhimurium*. *Proc. Natl Acad. Sci. USA* **109,** 18395–18400 (2012).
23. Qin, L. *et al.* Sialin (SLC17A5) functions as a nitrate transporter in the plasma membrane. *Proc. Natl Acad. Sci. USA* **109,** 13434–13439 (2012).
24. Harlow, E. & Lane, D. *Antibodies: A Laboratory Manual* (Cold Spring Harbor Laboratory Press, 1988).

Supplementary Information is available in the online version of the paper.

Acknowledgements We thank E. McCleskey for critically reading this manuscript and for discussions. We thank D. Cawley for development and production of monoclonal antibodies, and staff at the Advanced Light Source, Lawrence Berkeley National Laboratory for assistance with X-ray data collection. The Advanced Light Source is supported by the Director, Office of Science, Office of Basic Energy Sciences, of the US Department of Energy under Contract no. DE-AC02-05CH11231. Research in the Gonen laboratory is funded by the Howard Hughes Medical Institute.

Author Contributions H.Z. and T.G. designed the project. H.Z. performed all biochemical experiments including cloning, expression, purification, antibody production and binding assays, crystallization and X-ray data collection for both apo- and nitrite-bound NarK. H.Z. and G.W. built and refined the structures. All authors participated in data analysis and figure preparation. H.Z. and T.G. wrote the manuscript.

Author Information Structures of substrate-free and nitrite-bound NarK have been deposited in PDB under accession numbers 4JR9 and 4JRE, respectively. Reprints and permissions information is available at www.nature.com/reprints. The authors declare no competing financial interests. Readers are welcome to comment on the online version of the paper. Correspondence and requests for materials should be addressed to T.G. (gonent@janelia.hhmi.org).

METHODS

Protein expression and purification. The gene encoding full-length NarK from *E. coli* strain K12 was subcloned into pET15b (EMD Millipore) with a modified N-terminal 8× His-tag and a thrombin cleavage site. NarK was overexpressed in *E. coli* BL21 (DE3) C41 at 37 °C for 4–5 h with 0.3 mM IPTG as inducer. After induction, the cells were collected by centrifugation and resuspended in lysis buffer containing 20 mM Tris-HCl (pH 8), 150 mM NaCl and 1 mM PMSF. The resuspension was then passed through a microfluidizer (Microfluidics Corporation) twice at ~15,000 p.s.i., followed by centrifugation at 15,000*g* for 30 min. The supernatant was collected and centrifuged at 130,000*g* for 1 h. The pellets containing membrane were resuspended in the same lysis buffer and frozen at −80 °C until use.

To purify NarK, an aliquot of frozen membrane was thawed and solubilized with 1% *n*-decyl-β-D-maltopyranoside (DM) at 4 °C for 2 h. After addition of 20 mM imidazole followed by centrifugation, the supernatant was applied to Ni^{2+} nitrilotriacetate affinity resin (Ni-NTA). The resins were washed with 50 mM imidazole in the buffer containing 20 mM Tris-HCl (pH 8), 150 mM NaCl, 0.2% DM. Full-length NarK was then eluted with 250 mM imidazole in the same buffer. The His-tag was removed by thrombin digestion at an enzyme:protein molar ratio of 1:1,000 at 4 °C overnight. The enzyme-treated protein was further purified by gel filtration (Superdex-200) in 20 mM Tris-HCl (pH 8), 150 mM NaCl and 0.2% DM. NarK in the peak fractions was collected.

Fab production. Standard protocol[24] was used to generate the mouse IgG monoclonal antibodies against NarK. Western blot and native ELISA was performed to assess the binding affinity and specificity of the antibodies generated from hybridoma cell lines. Several monoclonal antibodies with strongest binding affinity were then purified from the hybridoma supernatants by protein A affinity chromatography. Fab was produced by papain digestion and purified by protein A affinity chromatography.

Assembly of NarK–Fab complex. Purified NarK and Fab were mixed at a molar ration of 1:2, and incubated at 4 °C for 30 min. The complex was then concentrated and purified by gel filtration chromatography with 20 mM Tris-HCl (pH 8), 150 mM NaCl and 0.2% DM. A clear and complete peak shift to higher molecular weight was observed, indicating homogeneous NarK–Fab complex formation. The purified protein complex was collected and concentrated to 5.8 mg ml^{-1}.

Crystallization. Initial hanging-drop crystallization assay with purified NarK produced crystals grown in a large range of crystallization condition with PEG molecules. However, these crystals gave anisotropic diffraction to around 4 and 6 Å. High-quality crystals were obtained only when NarK was co-crystallized as a complex with Fab. The best crystal, which diffracted to ~2.5 Å, was obtained with Fab prepared from hybridoma line 4G5 (IgG2a, kappa) in the following precipitant condition: 0.1 M citric acid (pH 3.5), 0.1 M NaCl, 0.1 M Li_2SO_4 and 28% PEG400. Before data collection, the crystals were soaked in a cryoprotectant buffer containing 30% PEG400 in the same precipitant solution for 5 min, and rapidly frozen in liquid nitrogen. For soaking, the NarK crystals were transferred into a precipitant solution containing 50 mM sodium nitrite or sodium nitrate overnight, and then frozen as above. Nitrite-bound-NarK crystals diffracted to ~2.8 Å resolution.

Data collection and structure determination. The data sets were collected at the Advanced Light Source (beamline 8.2.2), and processed with HKL2000[25] to 2.6 Å (substrate-free NarK) and 2.8 Å (nitrite-bound NarK) resolution. Further structure determination and refinement were accomplished using the CCP4 package[26].

The structure was determined by molecular replacement using the program Phaser[27] with a polyalanine Fab fragment derived from the Protein Data Bank (PDB ID 1F8T[28]) as a search model. Phases from molecular replacement were significantly improved after cycles of density modification using the program Parrot[29], and the electron density for the 12 transmembrane helices became apparent. Manual model building was carried out for the Fab using the program Coot[30], followed by structure refinement using the program Refmac[31]. To facilitate model building of NarK, 20-residue polyalanine helices were placed in the asymmetric unit by molecular replacement. Subsequent cycles of density modifications, model building and refinement were carried out until structure completion. The final model contains one molecule of NarK (residues 12–458) and one molecule of the heavy and light chains of the Fab in the asymmetric unit. Data collection and refinement statistics are presented in Supplementary Table 1.

All figures in this paper were prepared with Chimera version 1.6.2[32] or Pymol version 1.5[33] and assembled in Photoshop CS6 (Adobe). Supplementary Fig. 2 was prepared using the program Clustal X[34].

25. Otwinowski, Z. & Minor, W. Processing of X-ray diffraction data collected in oscillation mode. *Methods Enzymol.* **276,** 307–326 (1997).
26. Winn, M. D. *et al.* Overview of the CCP4 suite and current developments. *Acta Crystallogr. D* **67,** 235–242 (2011).
27. McCoy, A. J. *et al.* Phaser crystallographic software. *J. Appl. Crystallogr.* **40,** 658–674 (2007).
28. Fokin, A. V. *et al.* Spatial structure of a Fab-fragment of a monoclonal antibody to human interleukin-2 in two crystalline forms at a resolution of 2.2 and 2.9 angstroms [in Russian with English abstract]. *Bioorg. Khim.* **26,** 571–578 (2000).
29. Zhang, K. Y., Cowtan, K. & Main, P. Combining constraints for electron-density modification. *Methods Enzymol.* **277,** 53–64 (1997).
30. Emsley, P. & Cowtan, K. Coot: model-building tools for molecular graphics. *Acta Crystallogr. D* **60,** 2126–2132 (2004).
31. Murshudov, G. N., Vagin, A. A. & Dodson, E. J. Refinement of macromolecular structures by the maximum-likelihood method. *Acta Crystallogr. D* **53,** 240–255 (1997).
32. Pettersen, E. F. *et al.* UCSF Chimera–a visualization system for exploratory research and analysis. *J. Comput. Chem.* **25,** 1605–1612 (2004).
33. The PyMOL Molecular Graphics System, Version 1.2r3pre, Schrödinger, LLC http://www.pymol.org/.
34. Larkin, M. A. *et al.* Clustal W and Clustal X version 2.0. *Bioinformatics* **23,** 2947–2948 (2007).